International Journal of Nanomedicine

Dovepress
open access to scientific and medical research

Open Access Full Text Article

ORIGINAL RESEARCH

Graphene Oxide/Gelatin Nanofibrous Scaffolds Loaded with N-Acetyl Cysteine for Promoting Wound Healing

Qian Yu[1,*], Chentao Shen[2,3,*], Xiangsheng Wang[4], Zhenxing Wang[5,6], Lu Liu[2,3], Jufang Zhang[4]

[1]Research Center, Plastic Surgery Hospital, Chinese Academy of Medical Sciences and Peking Union Medical College, Beijing, 100144, People's Republic of China; [2]Department of Gastrointestinal Surgery Center, Tongji Hospital, Tongji Medical College, Huazhong University of Science and Technology, Wuhan, 430030, People's Republic of China; [3]Cancer Research Institute, Tongji Hospital, Tongji Medical College, Huazhong University of Science and Technology, Wuhan, 430030, People's Republic of China; [4]Department of Plastic Surgery, Affiliated Hangzhou First People's Hospital, Zhejiang University School of Medicine, Hangzhou, 310006, People's Republic of China; [5]Department of Plastic Surgery, Union Hospital, Tongji Medical College, Huazhong University of Science and Technology, Wuhan, 430022, People's Republic of China; [6]Wuhan Clinical Research Center for Superficial Organ Reconstruction, Wuhan, 430022, People's Republic of China

*These authors contributed equally to this work

Correspondence: Jufang Zhang; Lu Liu, Tel +86-18800293916; +86-13476226821, Fax +86-571-87914773; +86-27-83662640, Email doctorzjf@zju.edu.cn; halesan@163.com

Purpose: We aimed to develop an antioxidant dressing material with pro-angiogenic potential that could promote wound healing. Gelatin (Gel) was selected to improve the biocompatibility of the scaffolds, while graphene oxide (GO) was added to enhance their mechanical property. The loaded N-Acetyl cysteine (NAC) was performing the effect of scavenging reactive oxygen species (ROS) at the wound site.

Materials and Methods: The physicochemical and mechanical properties, NAC releases, and biocompatibility of the NAC-GO-Gel scaffolds were evaluated in vitro. The regeneration capability of the scaffolds was systemically investigated in vivo using the excisional wound-splinting model in mice.

Results: The NAC-GO-Gel scaffold had a stronger mechanical property and sustainer NAC release ability than the single Gel scaffold, which resulted in a better capacity for cell proliferation and migration. Mice wound-splinting models revealed that the NAC-GO-Gel scaffold effectively accelerated wound healing, promoted re-epithelialization, enhanced neovascularization, and reduced scar formation.

Conclusion: The NAC-GO-Gel scaffold not only promotes wound healing but also reduces scar formation, showing a great potential application for the repair of skin defects.

Keywords: gelatin, graphene oxide, electrospinning, NAC, wound healing

Introduction

The increasing number of surgical procedures and the global prevalence of chronic wounds caused by diseases (such as cancer and diabetes) and chronic injuries (such as venous leg ulcers and pressure ulcers) have paralleled the demand for better wound healing processes.[1,2] The wound healing process broadly consists of four phases: (i) hemostasis, (ii) inflammation, (iii) proliferation, and (iv) maturation.[3] Hemostasis, the first phase of wound healing, begins at the onset of injury and only lasts for a few minutes, while the maturation phase varies significantly from wound to wound and can last for several months.[4–6] Minimizing scarring while accelerating the wound healing process are the current hotspots of wound healing research.

Oxidative stress is a series of adaptive responses caused by the imbalance between pro-oxidants and antioxidants, with an increase in the release of free radicals and/or a decrease in the antioxidant capacity of the body tissues.[7,8] Several cells produce free radicals, such as reactive oxygen species (ROS), to varying degrees during the wound healing process. ROS plays a pivotal role in the coordination of the normal wound healing response, such as regulating angiogenesis at the wound site and

Received: 17 October 2022
Accepted: 3 January 2023
Published: 1 February 2023

perfusing blood into the wound area.[9] However, excessive ROS can lead to tissue damage, often in chronic, unhealed wounds, which is detrimental to wound repair.[10]

An ideal wound dressing should optimize the microenvironment for the healing process, which included promoting hemostasis, maintaining suitable moist conditions, and providing pressure as well as barriers.[11–14] With the increasing need for wound dressings on the market, the novel bioactive wound dressing has become a research hotspot in the field of biomaterials. Collagen is a structurally and functionally vital extracellular matrix protein that participates in scar formation during the healing of connective tissues. Gelatin (Gel) is a mixture of peptides and proteins produced by physical, chemical, or enzymatic hydrolysis of collagen. As a natural macromolecule, gelatin is the best building blocks for the creation of wound dressings and biomaterials for skin regeneration.[15] The porous matrix of gelatin could absorb wound exudates and maintain a moist environment, which accelerates the wound healing process.[16] Several studies have shown that gelatin matrices act as a bioactive material for cell migration and provide structural support for the development of new tissue.[17,18] In addition, gelatin-based biomaterials could be used as a drug delivery system for specific therapeutic molecules.[19–21] However, the poor mechanical properties of gelatin dressings limit their wide application.

Several hybrid formulations have been developed to overcome the shortcoming of gelatin biopolymers, particularly the poor mechanical property. Graphene oxide (GO) is the oxidized form of graphene obtained by exfoliation and oxidation of graphite.[22] It has a high Young's modulus (~1.0 TPa) and good electrical conductivity that merit attention for biomedical applications.[23,24] Moreover, the chemical properties of GO can be modified, expanding its possible application for biomaterial research.

Many recent studies have focused on gelatin and the hybrid formulation of GO to obtain an optimal regenerative system. Nair et al[25] developed a 3D GO-reinforced gelatin-hydroxyapatite (GHA) scaffolds for bone regeneration. The addition of GO significantly enhances the mechanical strength of the GHA matrix and improves the level of osteogenic differentiation of human adipose-derived mesenchymal stem cells. Paul et al[26] developed an injectable hydrogel using methacrylated gelatin and GO nanocomplexes for vasculogenesis and cardiac repair. In vivo studies revealed that injection of this nanocomplex combined with the Vascular Endothelial Growth Factor (VEGF) significantly increased the myocardial capillary density in the infarcted region. Jiao et al[27] evaluated the impact of gelatin-reduced graphene oxide (GOG) on bone remodeling. The GOG manifested good biocompatibility, degradation, and enhanced osteoclastogenesis in bone marrow stromal stem cells in vitro. The effects of GOG on osteoclastogenesis and angiogenesis were also verified in the mouse orthodontic tooth movement model. Recent study revealed that GO-Gel scaffolds could enhance intestinal wall defect repair.[28] The GO-Gel scaffold exhibited good biocompatibility and promoted neovascularization. Therefore, these results strongly suggest that GO-Gel hybrid scaffolds could potentially be used for treating wounds and skin regeneration.

As an inhibitor of ROS, N-acetylcysteine (NAC) has been used for several decades in therapeutic practices.[29] NAC is a reduced glutathione (GSH) precursor and could easily enter the cell for its low molecular weight. NAC deacetylation produces cysteine, which promotes GSH synthesis even in an oxidative stress environment.[30] Oguz et al[31] compared the efficacy of dexpanthenol with 3% NAC for wound healing using a rat model. After 21 days, wound histological assessments showed that the NAC group has a significantly higher angiogenesis rate than other groups despite similar wound healing rates. Tsai et al[32] demonstrated that NAC improved re-epithelialization in the burn wound by activating wound healing signaling pathways. The CCD-966SK cells treated with NAC had been proved to have better cell viability and migration ability evaluated by MTT assay and scratch wound healing experiments in vitro. Overall, the above findings demonstrate the potentially wide application of NAC in skin tissue engineering.

In this study, we electrospun GO-Gel scaffolds and cross-linked them with NAC for wound healing research (Figure 1). The surface structure, physiochemical properties, NAC release ability, and biocompatibility were evaluated in vitro. Furthermore, the regenerative effect of scaffolds on defected skin was investigated using a mouse splint model.

Materials and Methods

Preparation of NAC-GO-Gel Nanofibrous Scaffolds

Gelatin was obtained from Macklin Biochemical Co. (Shanghai, China). Dissolving agent Hexafluoroisopropanol (HFIP), coupling reagents N-(3-Dimethylaminopropyl)-N'-ethylcarbodiimide hydrochloride (EDC) and N-Hydroxysuccinimide (NHS) were obtained from Aladdin Reagent Co. (Shanghai, China).

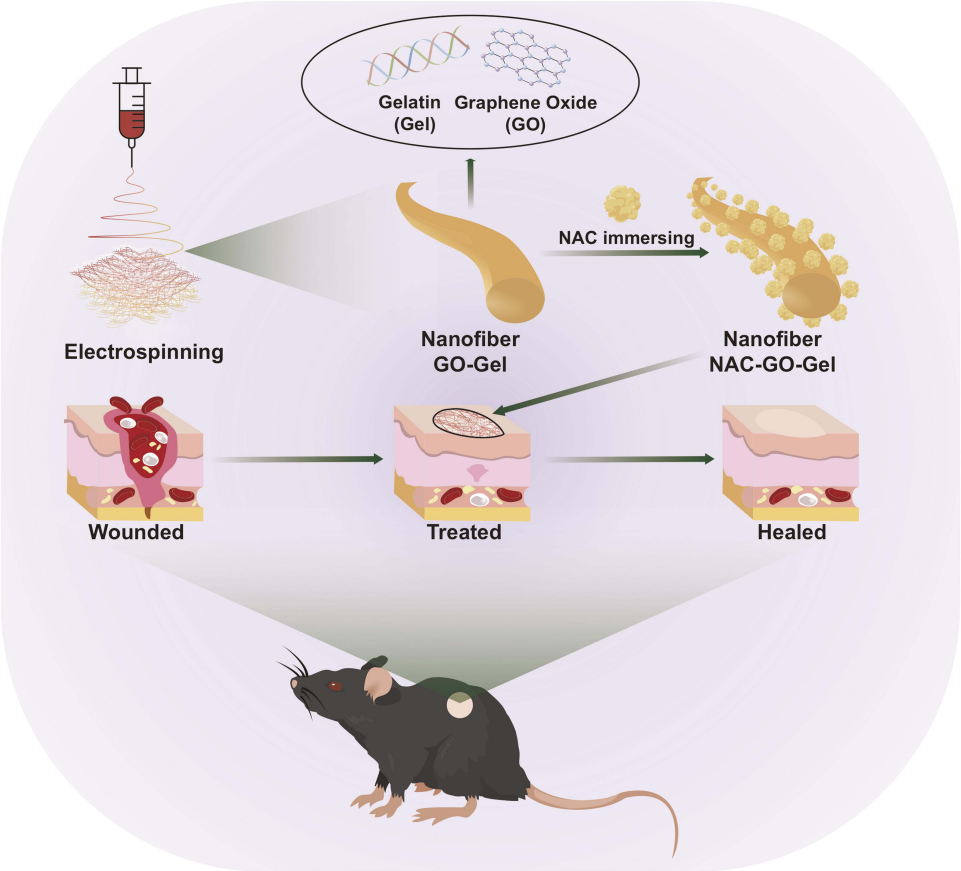

Figure 1 Schematic diagram for the experimental design. A blend of Gel and GO was firstly electrospun to fabricate the GO-Gel scaffold. Then, the GO-Gel scaffold was immersed in NAC-EDC/NHS solution and crosslinked to obtain the NAC-GO-Gel scaffold. The NAC-GO-Gel scaffold was subsequently applied to the mice's wound.

Firstly, gelatin was dissolved in HFIP to obtain a concentration of 50% w/v via continuous magnetic stirring for 24 hours. GO was prepared using a modified Hummer's Method as previously described.[33] Subsequently, GO was dispersed homogeneously in deionized water by ultra-sonication for 4 hours in an ice-cold water bath. Different volumes of GO dispersion were added to Gel/HFIP solution and stirred in an ice-cold water bath to obtain 0 and 25% w/v GO-Gel solution.

Secondly, the electrospun nanofibrous scaffolds were generated. Briefly, the GO-Gel solution was filled in a 5-mL syringe with a 19-gauge needle. The syringe was placed vertically, and the distance between the tip of the syringe needle and the collector was 20 cm. Electrospinning was then performed for 10 hours at 18 KV and a supply flow rate of 0.5 mL/h.

Thirdly, NAC-EDC/NHS solution was obtained by a mixture of 5% w/v EDC and 2% w/v NHS in 95% alcohol solution containing 0.1 mg/mL NAC. Then, the nanofibrous scaffolds (Gel, 0.25%GO-Gel) were crosslinked by immersing in NAC-EDC/NHS for 24 hours at room temperature. Finally, the scaffolds (Gel, NAC-Gel, GO-Gel, NAC-GO-Gel) were rinsed in distilled water and dried overnight in a vacuum oven.

Physiochemical Characterization of the NAC-GO-Gel Nanofibrous Scaffolds

Morphology of the Scaffolds

The scaffolds were coated with platinum before observation. The microstructure of scaffolds was then observed by a field emission scanning electron microscope (FESEM, Nova NanoSEM, Netherlands) at an accelerating voltage of 10 kV. The diameter of nanofibers was calculated using representative images in OriginPro 9 Software.

Surface characteristics of the scaffolds were recorded using an FTIR spectrometer (Thermo Scientific, Nicolet iS50R, Waltham, America) and a Raman spectrometer (LabRAM, HR800, Horiba JobinYvon, France). FTIR was measured at a resolution of 4 cm^{-1} in the frequency range of 400–5000 cm^{-1}, while the Raman spectra analysis was performed using a scanning range of 100–4000 cm^{-1}. The excitation source was a 30 mW diode laser with a 532 nm wavelength. The

X-ray diffraction (XRD) analysis was determined using an X-ray diffractometer (XRD, Empyrean, Netherlands) with Cu-Kα radiation in the range of 5°–90° (2θ).

Mechanical Properties of the Scaffolds

The mechanical properties of scaffolds were determined using an all-electric dynamic test instrument (Instron, British) equipped with a load cell capacity of 100 N and tensile speed of 10 mm/min. The stress–strain curve was plotted by GraphPad Prism 8 Software, and Young's modulus was calculated by OriginPro 9 Software.

In vitro NAC Release Test

Four NAC-Gel and NAC-GO-Gel scaffolds were immersed in 2 mL of PBS at 37°C. The soaking solution was filtered and transferred for subsequent tests at one, two, four, and eight hours, and one, three, seven, and 14 days. The released NAC concentration was measured using high-performance liquid chromatography (HPLC) as previously described.[34]

Biocompatibility of the Scaffolds in vitro

Cytological experiments were performed using human dermal fibroblasts (HDFs, ATCC, America). The cell culture process was carried out as previously described.[35] The Gel, NAC-Gel, GO-Gel, and NAC-GO-Gel scaffolds were cut into 5 mm square shapes and sterilized with ethylene oxide at 37°C overnight. The sterilized scaffolds were then placed at the bottom of 96-well culture plates and washed thrice with sterile PBS. Each well was seeded with 2×10^3 cells.

Cell Viability

The cell viability on scaffolds was measured using Calcein-AM (CAM) and Propidium iodide (PI) staining (Beyotime, China), performed after one, three, and seven days of cell culture. The cytoplasm of live and dead cells was stained green and red respectively by the CAM and PI. The fibroblasts were observed under a confocal laser scanning microscope (IX8 Olympus, Japan).

Cell Morphology

HDFs seeded on scaffolds were used for field emission scanning electron microscopy (FESEM) observation. After incubation for two days, HDFs on scaffolds were washed with PBS and fixed with 4% paraformaldehyde. The scaffolds were then dehydrated using graded ethanol and dried in air. Observation of cell adhesion and morphology was according to the above procedure.

Cell Proliferation

The proliferation of cells on the scaffolds was determined using Cell Counting Kit-8 (Beyotime, China) after incubation for 1–7 days of incubation. Briefly, 10 μL CCK-8 solution was added into 100 μL complete DMEM per well and incubated at 37°C for two hours. Subsequently, 100 μL of the supernatant solution was transferred to a new 96-well culture plate, and the optical density (OD) of the solution was measured at 450 nm using a microplate reader (BioTek ELx800, America).

Cell Migration

HDFs were seeded at a density of 2.5×10^5 cells per well in 6-well culture plates and cultured until 85–90% confluence. Scratches were drawn in the middle of wells using sterile 200 μL pipette tips. HDFs were then washed thrice with PBS and refilled with different extract mediums (complete DMEM in which scaffolds were immersed at 37°C for 24 hours). The images were captured using an optical microscope (Nikon ECLIPSE TS100, Japan) at 0, 12, and 24 hours after scratching.

In vivo Study on Mice Wound Splinting Models

All animal experiments and procedures were carried out in compliance with the guidelines of Plastic Surgery Hospital, and approved by the Animal Ethics Committee of the Plastic Surgery Hospital, Chinese Academy of Medical Sciences

and Peking Union Medical College. Twenty female C57BL/6J mice (age:7–9 weeks) were housed separately in a standardized environment. Mice were anesthetized by intraperitoneal injection of pentobarbital sodium at a dosage of 30 mg/kg. The dorsal region was shaved and sterilized with povidone-iodine and alcohol pads. The mouse wound splinting model was conducted as previously described.[36,37] Briefly, a full-thickness wound was made on each side of the back using a 5-mm biopsy punch. The 40 wounds were randomly divided into four groups (n = 10): Gel, NAC-Gel, GO-Gel, and NAC-GO-Gel. An inner diameter of 7 mm splinting ring was fixed to the skin around the wound using four interrupted sutures of 6.0 nylon to prevent local skin contraction. Incisions were covered with Gel, NAC-Gel, GO-Gel, and NAC-GO-Gel scaffolds, and then dressed with sterile transparent films (Tegaderm, 3M, America). Wounds were wrapped using a self-adhering elastic bandage (Coban, 3M, America), and images were recorded at 0, 3, 7, 10, and 14 days for further evaluation. The wound closing area was measured at the above time points using Image-Pro Plus Software.

Histological Analysis and Immunohistochemistry Staining

All mice were sacrificed 14 days post-operation and tissues were fixed with 4% paraformaldehyde, and stained with Hematoxylin-Eosin (H&E) to observe the granulation and wound closure. Collagen deposition was assessed using Masson's Trichrome staining and Sirius Red staining. Furthermore, the expression of CD31 was analyzed using immunohistochemistry staining to evaluate neovascularization. The number of new vessels was measured using Image-Pro Plus Software.

Real Time-PCR Analysis

Skin tissues of the wound area were excised at 14 days post-operation to determine the relative mRNA expression level of various genes. The primer sequences of genes are listed in Table 1.

Statistical Analysis

Data were expressed as the mean value ± standard deviation from at least triplicate samples. Statistical analysis was performed using GraphPad Prism 8 Software. Differences between groups were analyzed using Student's t-tests and one-way ANOVA. All data are represented as mean ± SD, and P value <0.05 was considered to be statistically significant.

Results

Morphology and Physicochemical Characterization of the Scaffolds

The Gel, NAC-Gel, GO-Gel, and NAC-GO-Gel scaffolds showed different colors, in which the Gel scaffold was white while the GO-Gel scaffold was light brown (Figure 2A). The transmission electron microscopy (TEM) of GO is presented in Figure S1A. Scanning electron micrographs of scaffolds revealed that the addition of GO and NAC had no effect on the formation of electrospinning nanofibers. The NAC-GO-Gel nanofiber was distributed randomly and uniformly to form a three-dimensional mesh structure that closely simulated the human extracellular matrix. It can also be observed that interlaced pores cover most of the scaffolds, which character is suitable for biomedical applications.

The histogram of fiber diameter distribution in each scaffold is presented in Figure 2B. The mean fiber diameters of the Gel, NAC-Gel, GO-Gel, and NAC-GO-Gel scaffolds were 1050±84 nm, 1018±73 nm, 748±69 nm, and 753±80 nm, respectively. The addition of GO decreased the fiber diameter, while the external NAC coating had no effect on the fiber diameter.

The molecular structure and chemical composition of different groups of scaffolds were investigated to identify chemical changes in the GO-Gel scaffolds during the electrospinning process, FTIR spectra of different scaffolds are shown in Figure 2C. Gel, and the GO-Gel scaffolds exhibited similar FTIR spectra, in which the absorption peak of amide A, amide I, amide II, and amide III occurred at 3286 cm^{-1}, 1631 cm^{-1}, 1535 cm^{-1}, 1240 cm^{-1}, respectively. Besides, GO exhibited the characteristic peaks at 1732 cm^{-1} (carboxylic acid C=O stretching), 1613 cm^{-1} (C=C stretching), 1227 cm^{-1} (C-OH stretching) and 1052 cm^{-1} (C-O stretching) (Figure S1B). Due to the weak infrared

Table 1 Quantitative Real-Time PCR Primers

Gene Name	Sequence
GAPDH forward	5′-CCTCGTCCCGTAGACAAAATG −3′
GAPDH reverse	5′-TGAGGTCAATGAAGGGGTCGT-3′
ACTA2 forward	5′-GTACCACCATGTACCCAGGC-3′
ACTA2 reverse	5′-GAAGGTAGACAGCGAAGCCA-3′
COL1A1 forward	5′-GAGAGGTGAACAAGGTCCCG-3′
COL1A1 reverse	5′-AAACCTCTCTCGCCTCTTGC-3′
TIMP1 forward	5′-GCAACTCGGACCTGGTCATAAG-3′
TIMP1 reverse	5′-TCCCACAGCCTTGAATCCTTT-3′
MMP13 forward	5′-CTTCTTCTTGTTGAGCTGGACTC-3′
MMP13 reverse	5′-CTGTGGAGGTCACTGTAGACT-3′
VEGF forward	5′-GAGCGTTCACTGTGAGCCTTGT-3′
VEGF reverse	5′-TTAACTCAAGCTGCCTCGCCT-3′
TGF-β1 forward	5′-TAATGGTGGACCGCAACAAC-3′
TGF-β1 reverse	5′-CCACATGTTGCTCCACACTTGAT-3′
SMAD3 forward	5′-GGAATGCAGCCGTGGAACTT-3′
SMAD3 reverse	5′-TTGCAGCCTGGTGGGATCTT-3′
SMAD7 forward	5′-GGCCGGATCTCAGGCATTC-3′
SMAD7 reverse	5′-TTGGGTATCTGGAGTAAGGAGG-3′

absorption of GO, the characteristic infrared spectrogram of the GO-Gel scaffold was similar to that of Gel. Meanwhile, no NAC characteristic FTIR absorption peak for NAC groups was found.

Raman spectra of the scaffolds are analyzed in Figure 2D. The spectrum of the GO showed the characteristic peaks of the D band at 1356 cm^{-1} and the G band at 1604 cm^{-1} (Figure S1C). Meanwhile, the spectrum of the Gel scaffolds presented a smooth curve, while the scaffolds containing GO showed an M-shaped spectrum, indicating that GO was successfully incorporated into the GO-Gel scaffold. In scaffolds containing NAC, the Raman spectrogram showed a characteristic peak of 2943 cm^{-1}, indicating successful coating of scaffolds with NAC.

Figure 2E shows the XRD spectra of Gel, NAC-Gel, GO-Gel, and NAC-GO-Gel scaffolds. Obvious peaks around $2\theta=15°$ and $2\theta=22°$ were observed in the GO spectra (Figure S1D), which was in line with the previous study.[38] No diffraction peak was observed in any other scaffolds. The disappearance of GO diffraction peak indicated that GO powder was dispersed uniformly in GO-Gel scaffolds.

The mechanical strength, tensile strain, and Young's modulus of different scaffolds were further investigated to determine whether the addition of NAC and GO affects the mechanical strength of scaffolds. Figure 2F shows the stress–strain curves of different scaffolds which presented as basically linear within the 6% strain range. Tensile strains of GO-Gel and NAC-GO-Gel were significantly higher than that of Gel and NAC-Gel groups, owing to the aggregation of GO (Figure 2G). Moreover, Young's modulus of Gel, NAC-Gel, GO-Gel, and NAC-GO-Gel was calculated as the slope of the linear part of stress–strain curves, which was 23.61±1.90 MPa, 23.87±2.76 MPa, 87.82±4.43 MPa, and 94.13 ±3.25 MPa, respectively (Figure 2H). The aggregation of GO enhanced the mechanical strength of Gel scaffolds, and the addition of NAC had no significant effect on Young's modulus of the scaffold.

In vitro Biocompatibility of the Scaffolds

The biocompatibility of scaffolds was examined using CAM/PI staining. Live fibroblasts stained green with calcein-AM while dead fibroblasts stained red with propidium iodide. Compared to the NAC-Gel and Gel scaffolds, there was a slight increase in CAM fluorescence intensity in the NAC-GO-Gel and GO-Gel scaffolds after three days (Figure 3A). The intensity of CAM fluorescence on the NAC-GO-Gel scaffold was significantly higher than that of the other three scaffolds after seven days, consistent with the result of CCK8 assay (Figure 3C). The NAC-GO-Gel scaffold performed notably better cell viability and proliferation rates compared with Gel, NAC-Gel, and GO-Gel scaffolds. Furthermore, cell morphology and cell attachment on scaffolds were investigated using FESEM after two days of culture. The

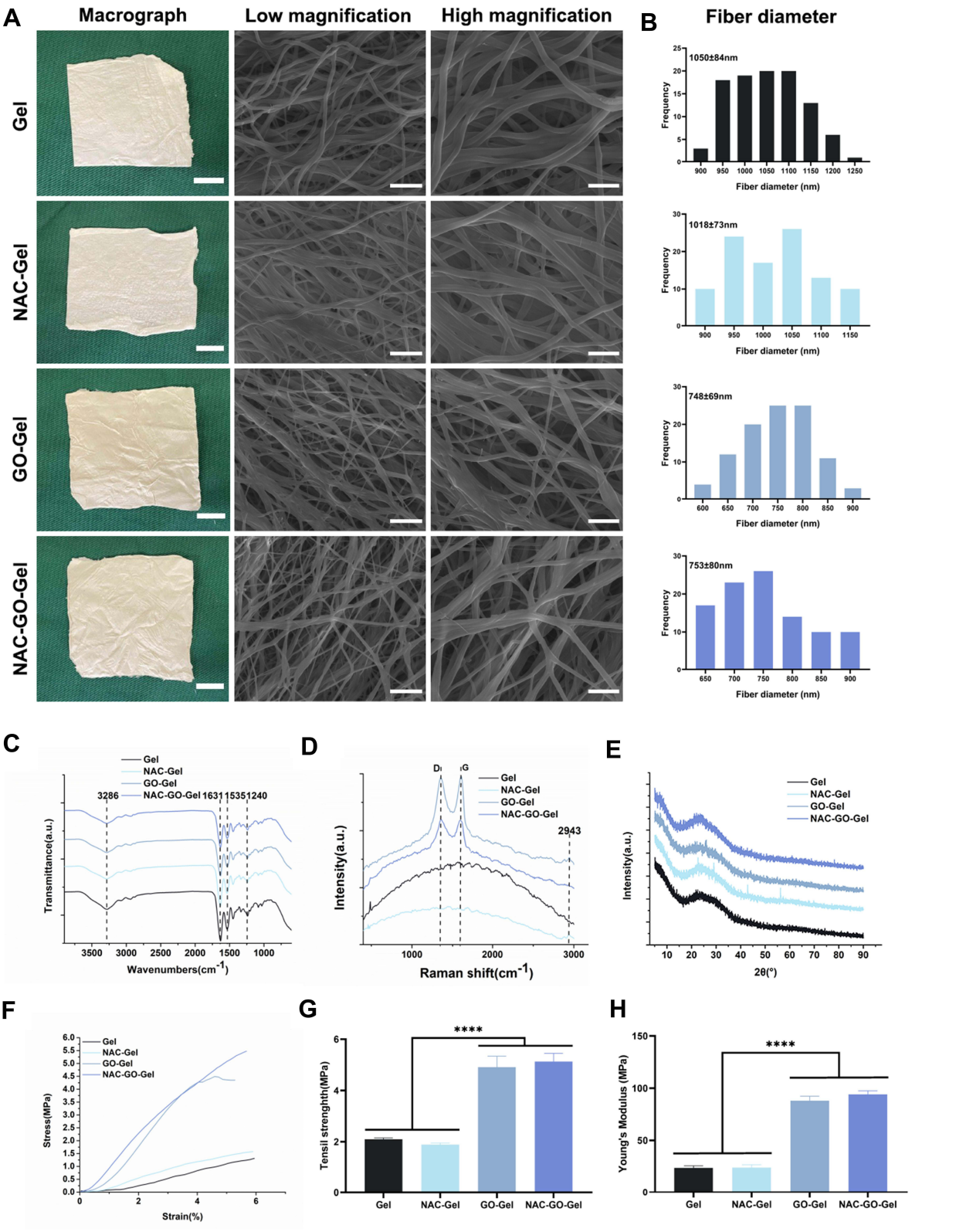

Figure 2 Characterization of NAC-GO-Gel nanofibrous scaffolds. (**A**) Macrographs and FESEM images (scale bar: low magnification=10 μm, high magnification=5 μm); (**B**) histograms of nanofibers' diameter distribution; (**C**) FTIR spectroscopy; (**D**) Raman spectroscopy; (**E**) XRD spectroscopy; (**F**) tensile stress–strain curves; (**G**) tensile strength, and (**H**) Young's modulus of the scaffolds (mean±SD, ****P <0.0001).

https://doi.org/10.2147/IJN.S392782 DovePress

fibroblasts showed successfully adhered to the scaffolds in which HDFs were colored in blue, while the scaffolds were colored in green (Figure 3B). Moreover, all the nanofibrous scaffolds showed excellent hemocompatibility (Figure S2). Overall, the NAC-GO-Gel scaffold presented good in vitro biocompatibility.

In vitro NAC Release

NAC release curves of NAC-Gel and NAC-GO-Gel scaffolds are shown in Figure 3D. Consistent with the previously described, NAC release process consisted of two stages.[28] For the first day, the most loaded NAC was released by NAC-

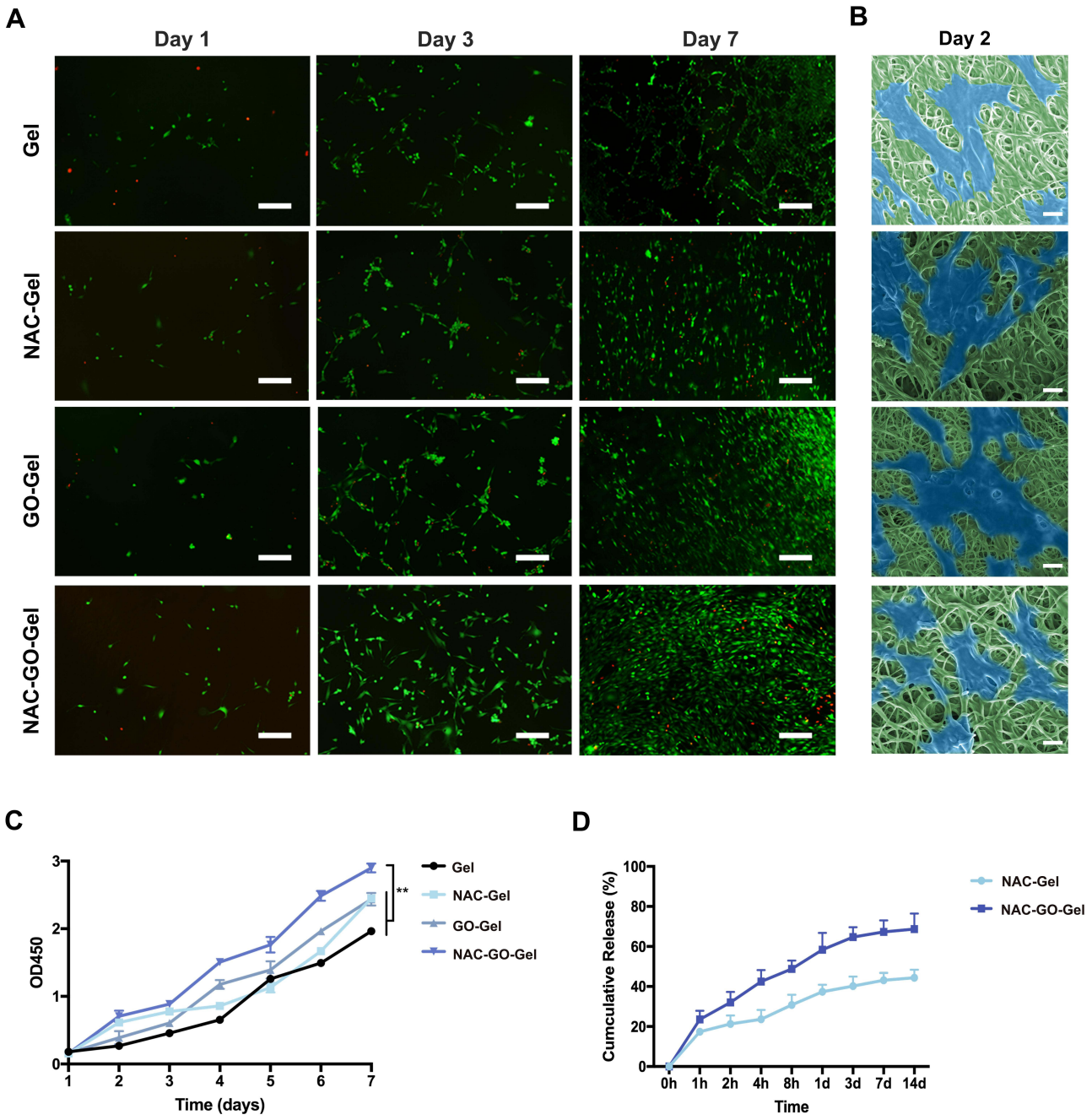

Figure 3 In vitro biocompatibility of the scaffolds. (**A**) Confocal fluorescent images for CAM/PI staining of human dermal fibroblasts on the scaffolds after 1, 3, and 7 days of culture (scale bar=200 μm); (**B**) FESEM images of human dermal fibroblasts on the scaffolds after two days of culture (scale bar=10 μm); (**C**) CCK8 assay results of human dermal fibroblasts seeded on the scaffolds. The fibroblasts had the best cell proliferation rates on the NAC-GO-Gel scaffold compared with other groups; (**D**) NAC release curve of NAC-Gel and NAC-GO-Gel scaffolds. The navy-blue curve shows that the NAC-GO-Gel had a sustainer drug release ability (mean ± SD, **P < 0.01).

Gel and NAC-GO-Gel scaffolds, and the release percentage was higher for the NAC-GO-Gel (58.4% ± 6.86%) than NAC-Gel (37.33% ± 2.90%). The second stage of NAC release occurred from day 1 to 14, and NAC release was more sustained in NAC-GO-Gel (68.68% ± 6.33%) than in NAC-Gel (44.4% ± 3.31%). Both GO and Gel are abundant with -COOH groups, which makes it possible to form an amide linkage with the -COOH of NAC.[39] Thus, the hybrid scaffold might have more linkage with NAC for more binding sites, resulting in a higher released amount of NAC in the NAC-GO-Gel scaffold than that in the NAC-Gel scaffold.

Cell Migration

Cell migration in Gel, NAC-Gel, GO-Gel, and NAC-GO-Gel scaffolds is shown in Figure 4A. HDFs migrated faster on the NAC-GO-Gel scaffold than that on the Gel, NAC-Gel, and GO-Gel scaffolds. The migration area was calculated using Image-Pro Plus software (Figure 4B). The percent of migration area in the NAC-GO-Gel group was 65.67% ± 4.92% in 12 hours and 89.67% ± 4.92% in 24 hours, significantly higher than that in Gel (18.13% ± 1.52% in 12 hours and 43% ± 7.26% in 24 hours), NAC-Gel (45.33% ± 4.11% in 12 hours and 60% ± 4.9% in 24 hours), and GO-Gel (37.33% ± 3.09% in 12 hours and 56.33% ± 3.86% in 24 hours) groups.

Mice Wound Healing Models

The wound healing models were covered with Gel, NAC-Gel, GO-Gel, and NAC-GO-Gel scaffolds separately to evaluate the wound healing effect of scaffolds in vivo. The wound healing process on day 0, 3, 7, 10, and 14 is shown in Figure 5A. Wound closure rates are calculated in Figure 5B. Before day 3, there was no difference in the percentages of wound closure areas in the four groups. The percentage of wound closure in the NAC-GO-Gel group (86.62% ± 6.23%) was notably higher than that in other groups on day 7. The Gel, NAC-Gel, and GO-Gel groups exhibited 30.13% ± 9.55%, 53.2% ± 6.61%, and 61.32% ± 4.69% wound closure, respectively. Most of the wounds in the NAC-GO-Gel group presented a wound closure on day 10, and re-epithelization was accomplished after 14 days. The wound closure rate on day 14 was higher in the of NAC-GO-Gel (99.21% ± 0.8%) group than in the Gel (82.4% ± 4.25%), NAC-Gel (91.53% ± 5.22%), and GO-Gel (93.14% ± 6.33%) groups. To sum up, the fastest wound closure rate among the four groups was observed in the NAC-GO-Gel group.

Histological Analysis and Immunohistochemistry Staining

HE staining of wound areas covered with four scaffolds is presented in Figure 6A. The areas without hair follicles and sebaceous glands were drawn between black dashed lines, indicating incomplete wound healing. Statistics of the length of incomplete wounds demonstrated that the NAC-GO-Gel group significantly enhanced wound healing (Figure 6C). Moreover, hair follicle formation in NAC-GO-Gel group was notably higher than other groups (Figure 6D).

Immunohistochemistry staining for CD31 was performed to investigate the effect of different scaffolds on the neovascularization process at the wound site (Figure 6B). The respective number of blood vessels at the wound site for each group is calculated in Figure 6E. Specifically, the wound area in the NAC-GO-Gel group had the most number of blood vessels, while the wound area in the Gel group had the least. The number of new blood vessels in the NAC-GO-Gel and NAC-Gel groups was almost twice those in the GO-Gel and Gel groups, suggesting that NAC notably enhanced neovascularization during the wound healing process.

The collagen regeneration process was examined using Masson's Trichrome staining (Figure 7A). On day 14, the collagen fibers in the NAC-GO-Gel group presented a more regular and uniform arrangement. In the meantime, the type of collagen fibers was investigated by Sirius red staining (Figure 7B) which was observed under a polarized light microscope. It was found that the most type of collagen fibers was type I collagen which presented as red in color. In addition, wounds in the NAC-GO-Gel group presented a more regular and well-organized collagen fiber arrangement and a decreased ratio of type I/III collagen, indicating that NAC-GO-Gel scaffolds reduced scar formation after wound healing.

The Expression of mRNA for Multiple Genes Using RT-PCR

The expression level of mRNAs for multiple genes in the wound tissue was examined by RT-PCR (Figure 7C) at day 14 days post-wounding. In accordance with the histological result of CD31 staining, VEGF mRNA expression in the NAC-GO-Gel group was remarkably higher than that in other groups. The mRNA expression level of fibrosis-related genes, including ACTA2

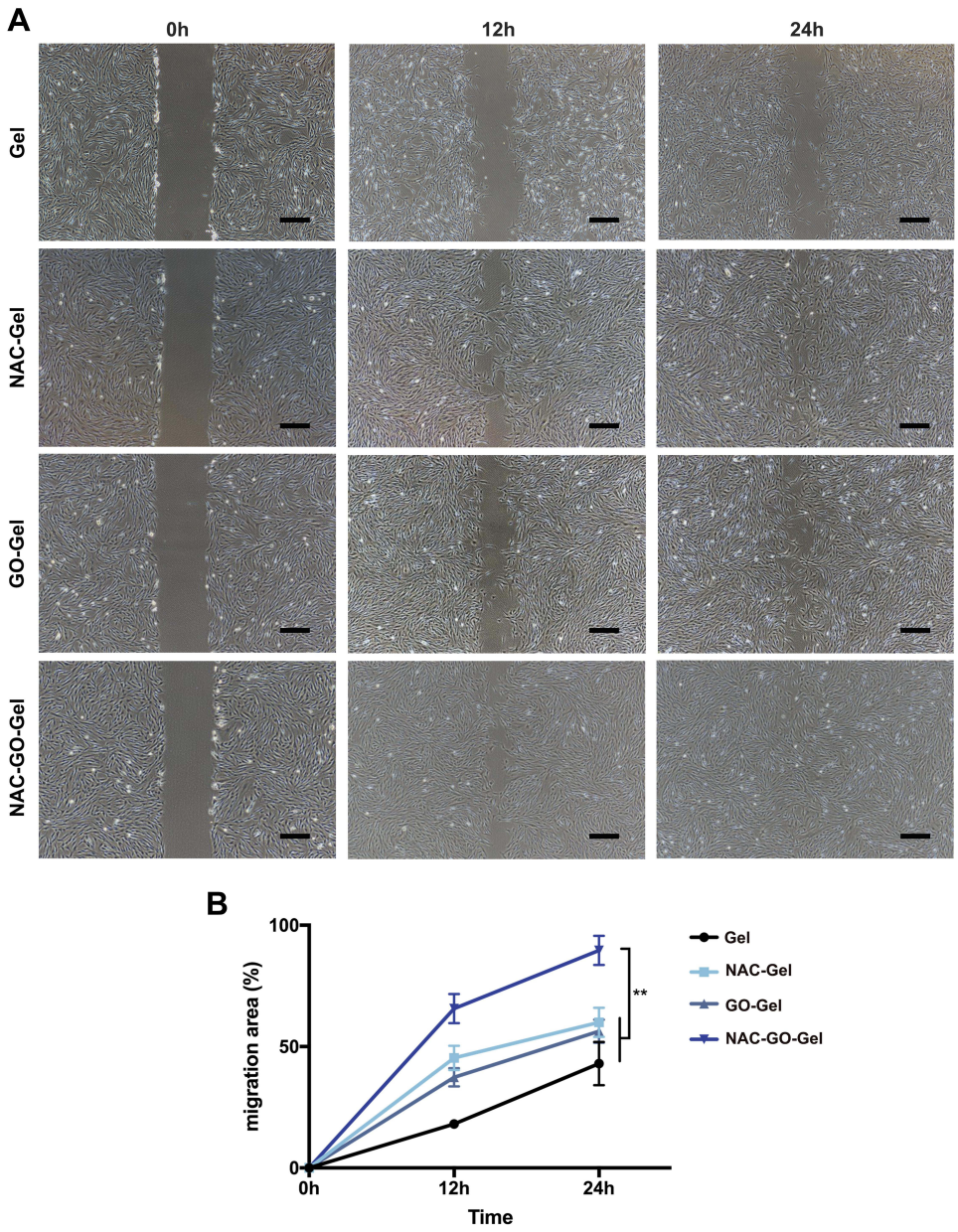

Figure 4 Scratch experiment of human dermal fibroblasts. (**A**) Scratch images of fibroblasts cultured by leaching four solutions of the scaffolds after 0, 12, and 24h (scale bars=400 μm); (**B**) migration area (%) of the fibroblasts in different scaffold groups (mean ± SD, **P < 0.01).

and COL1A1, was significantly suppressed in wound tissue of the NAC-GO-Gel group. Moreover, the expression level of key genes in TGFβ signaling, including TGF-β1 and Smad3, were downregulated in the NAC-GO-Gel group. The expression of extracellular matrix metabolism markers, including MMP13 and TIMP1, was increased and decreased respectively.

Discussion

Wound healing is a complex process, involving a variety of cellular events and natural responses to tissue injury. With the global growing number of surgical procedures and chronic wounds, promoting wound healing has been a major therapeutic challenge. This study presents a GO-Gel scaffold loaded with NAC for wound healing, which has good biocompatibility and pro-angiogenic capacity. Mouse wound models and in vitro experiments revealed that the NAC-GO -Gel scaffold enhances fibroblast proliferation and migration, accelerates wound healing, and promotes angiogenesis. In addition, fibrosis-related gene expression of wound tissue was remarkably downregulated resulting in a reduced scar formation.

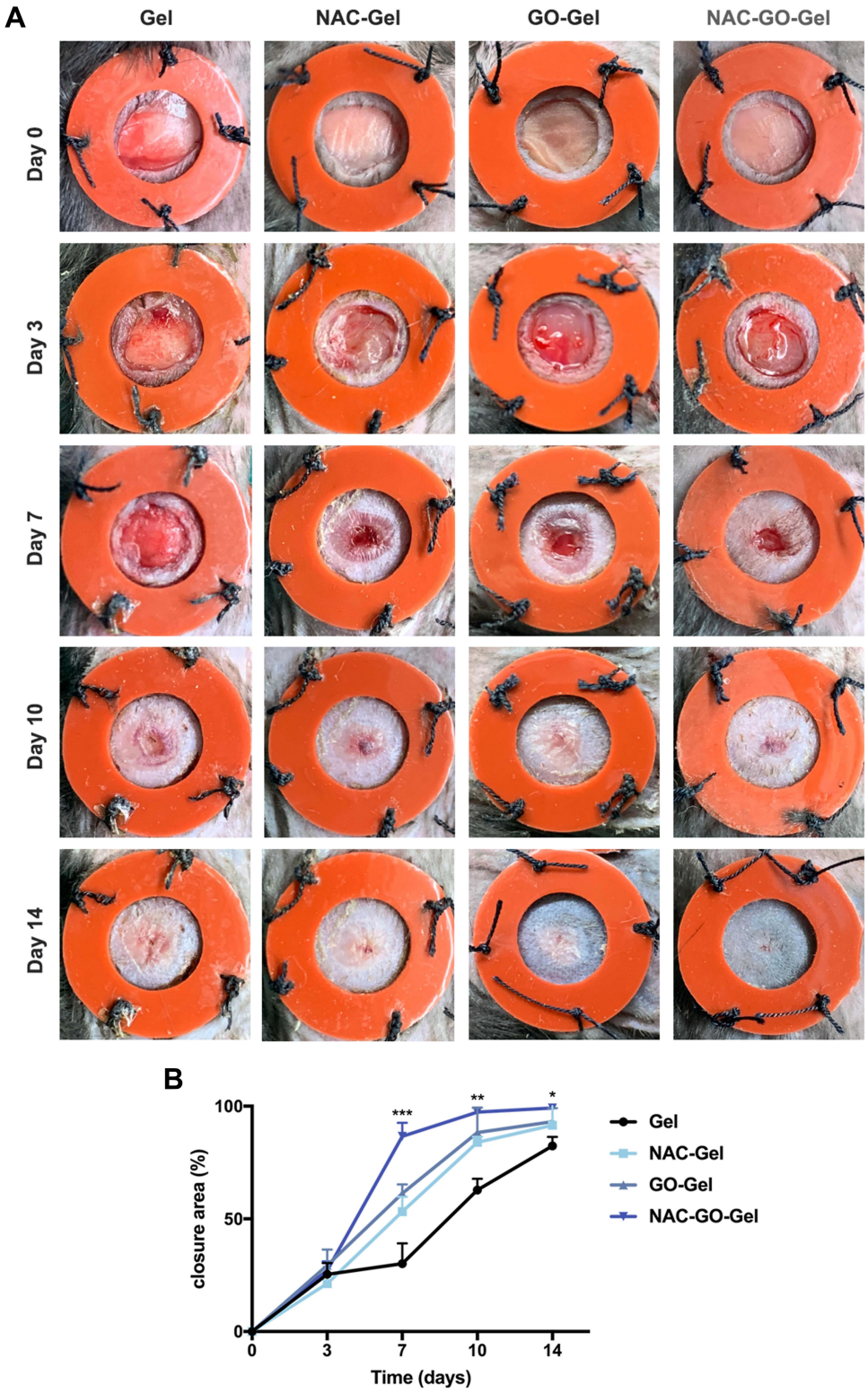

Figure 5 In vivo wound healing evaluation of Gel, NAC-Gel, GO-Gel, and NAC-GO-Gel scaffolds. (**A**) Photographic evaluation of wound repair in four groups on day 0, 3, 7, 10, and 14; (**B**) closure area (%) of the wound defect. NAC-GO-Gel group achieved the best effect among four groups on day 7, 10, and 14 (mean ± SD, ***P < 0.001, **P<0.01, *P<0.05).

An ideal wound dressing should effectively enhance and accelerate the healing process. Currently, biopolymer-derived electrospinning nanofibers have become a popular choice for wound dressing because of their excellent biocompatibility and good mechanical property.[40] Gelatin is a natural biopolymer derived from the hydrolysis of type

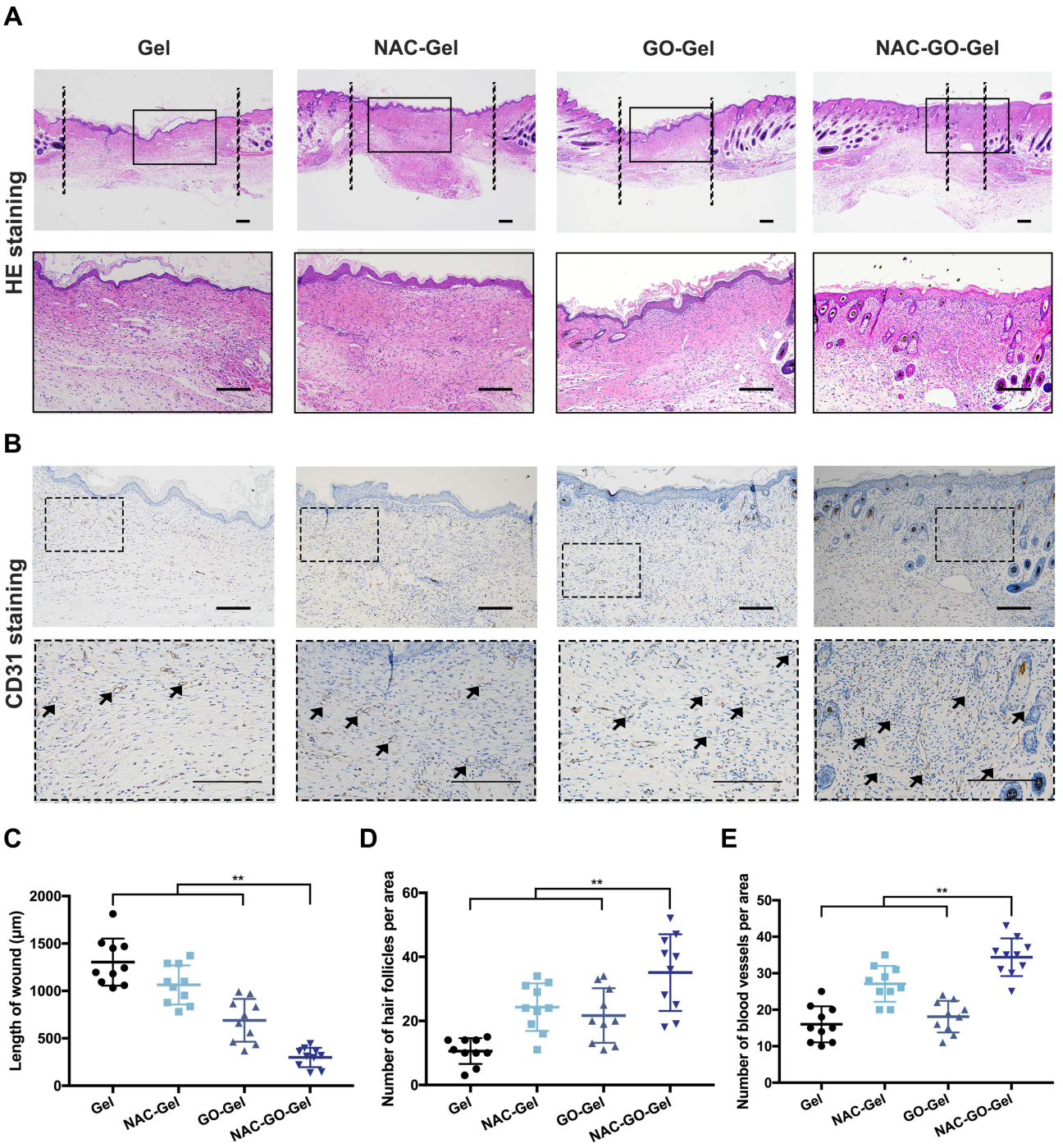

Figure 6 Histological analysis of wound tissues on day 14. (**A**) H&E staining of tissue sections. The area between black dash lines: incomplete wound healing, and high magnified views of the central area are within the black solid lines; (**B**) immunofluorescence images of CD31. The black arrows indicate new blood vessels; (**C**) length of the incomplete wound; (**D**) number of hair follicles per area and (**E**) number of new blood vessels per area (scale bars=100 μm; mean ± SD, **P < 0.01).

I collagen and exhibits excellent biocompatibility, low antigenicity, and controlled biodegradability, which make it a desirable candidate for wound dressings and tissue engineering.[15,41] However, the poor mechanical property of gelatin limits its wide application. Therefore, researchers continue to develop composite formulations by incorporating gelatin and other synthetic polymers to improve the mechanical properties of gelatin while enhancing the ability to release bioactive molecules.[42,43] Graphene oxide is a strong and flexible carbon-based compound. In addition, it can be chemically modified and has been widely used for biomedical applications in the last few years.[44] Incorporating GO

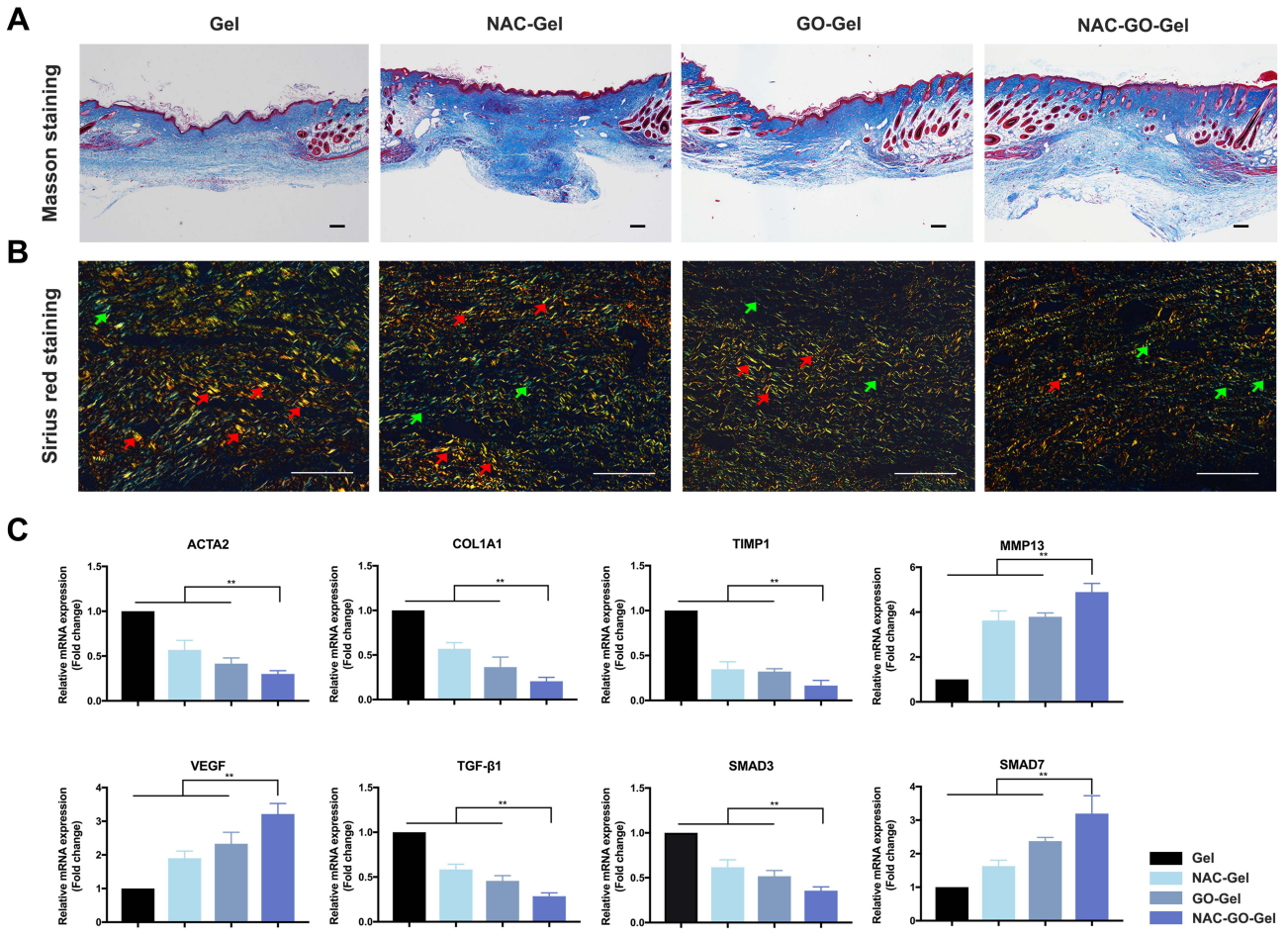

Figure 7 Collagen deposition and fibrotic genes expression of wound tissues on day 14. (**A**) Masson's Trichrome staining and (**B**) Sirius red staining of tissue sections (scale bars=100 μm), The red arrows and green arrows indicate the type I collagen and type III collagen, respectively. The NAC-GO-Gel group shows a remarkably decreased ratio of type I/III collagen which indicated a reduction of scar formation; (**C**) relative mRNA expressions of fibrosis-related genes 14 days post-wounding (mean ± SD, **P < 0.01).

with gelatin matrix can improve their mechanical properties and creates additional pore structures for better diffusion of nutrients and waste products.[26] Due to the excellent biocompatibility and robust physical properties, the combination formulation of gelatin and GO presents a viable choice for the fabrication of wound dressing.

Electrospinning technology allows for the production of fibers with nanometers, which character has various advantages in wound dressing fabrication since it resembles the natural extracellular matrix.[45] Additionally, the electrospinning scaffolds could provide sufficient air and water vapor permeability to allow oxygen in, which is also essential for wound healing. Ramanathan et al[46] extracted collagen from fish skin and employed to coat a scaffold based on poly (3-hydroxybutyric acid), gelatin and coccinia grandis extract through electrospinning. This nanofibrous scaffold accelerated rapid wound healing in a rat anti-inflammatory model through increasing the collagen deposition and reepithelialization. Singaravelu et al[47] fabricated a dual-layer 3D nanofibrous scaffold using poly (3-hydroxybutyric acid), gelatin and curcumin overlaid on a keratin-fibrin-gelatin sponge loaded with mupirocin for tissue engineering applications. The cytocompatibility of scaffold was tested on NIH 3T3 and HaCaT cells, and results showed that the dual-layer scaffold assisted in cell proliferation and adhesion. Moreover, the electrospun scaffold enhanced wound healing process in silicone splint animal model, presented as increased granulation tissue formation and collagen deposition. In this study, we prepared GO-Gel scaffolds using the electrostatic spinning method and assessed their mechanical property. The tensile strength and Young's modulus of GO-Gel scaffolds were considerably higher than those of single Gel scaffolds (Figure 2), indicating that the incorporation of GO effectively improved the mechanical strength of the scaffolds. With the increasing application of GO, its toxicity has been widely discussed.[48] Balanced tradeoffs between

the positive therapeutic effects of GO and the side effects associated with its toxicity should always be noted. Previous research analyzed the cell proliferation among different concentrations of GO within GO-Gel scaffolds, and results showed that low-concentration GO-Gel scaffold (0.25%) was better biocompatible.[28] Moreover, the 0.25% GO is degradable and promotes intestinal wall defect repair in vivo. Consistent with the previous finding, our results showed that cell viability and proliferation in the 0.25% GO-Gel group were significantly increased than in the Gel group (Figure 3), which might be due to the enhanced mechanical property.

Decreasing excessive ROS in surrounding environment is also an important factor for healing process except for providing good biocompatibility and robust mechanical strength. In our study, NAC was loaded on the GO-Gel scaffold to promote wound healing. As an antioxidant, topical application of NAC on skin defects inhibits oxidative stress and scavenges ROS at the skin wound site. Previous studies have demonstrated that topical application of NAC could promote angiogenesis, increase re-epithelialization, and improve local microcirculation in wound healing.[31,32] Bachle et al[49] revealed that topical application of NAC enhanced arteriolar perfusion and promoted angiogenesis in mice, reducing ischemia in all flap areas, consistent with our results. In the present study, in vitro experiments revealed that the incorporation of NAC (NAC-Gel group) promotes the migration of cells, and the addition of GO enhanced this process further (NAC-GO-Gel group) (Figure 4). Meanwhile, the NAC-GO-Gel group had the highest number of CD31-positive vessels (Figure 6) and the highest gene expression of the VEGF gene according to RT-PCR results (Figure 7C) in our mouse excisional wound healing model. Therefore, the NAC-GO-Gel scaffold enhances the release of NAC, reduces the production of ROS levels (Figure S3), and accelerates the migration and adhesion of fibroblast in the early stages of wound healing (Figure 5).

Progressive fibrosis during wound healing causes scarring, characterized by excessive extracellular matrix deposition and overexpression of fibrosis-related genes. Paskal et al[50] revealed that NAC dysregulated the expressions of numerous genes associated with scar formation and improved neovascularization. The present study revealed that NAC significantly downregulated the expression of mRNA for fibrosis-related genes (Figure 7). Wounds, particularly severe wounds with excessive tension or movement, are vulnerable to tissue infection, necrosis and other adverse effects during healing. The infection factor during wound healing process has been received extensive attention, and many wound dressings were developed to reduce microbial infection. However, the direct antimicrobial effect of the scaffolds was not the major purpose of this study. Our nanofibrous scaffolds presented to provide an excellent physiological background, and thus to promote wound healing process through enhancing cell proliferation and neovascularization. The NAC-GO-Gel scaffold improved the NAC release, promoting wound healing through enhanced neovascularization and reduced fibrotic scar formation.

Conclusions

In summary, we successfully developed NAC-loaded GO-Gel scaffolds as a novel dressing for skin wound repair. The NAC-GO-Gel scaffold exhibits a strong mechanical property, excellent biocompatibility, and sustained release ability of NAC, thus resulting in a promoted cell proliferation and migration in vitro studies, as well as rapid and scarless healing of a 5-mm mice's wound in vivo experiments.

Acknowledgments

This study was funded by the Construction Fund of Medical Key Disciplines of Hangzhou (grant. 0020200044), the Medical and Health Science and Technology Program of Hangzhou (grant. Z20200127 and grant. A20220646).

Disclosure

The authors report no conflicts of interest in this work.

References

1. Deshmukh S, Kathiresan M, Kulandainathan MA. A review on biopolymer-derived electrospun nanofibers for biomedical and antiviral applications. *Biomater Sci*. 2022;10(16):4424–4442. doi:10.1039/D2BM00820C

2. Grip J, Engstad RE, Skjaeveland I, et al. Beta-glucan-loaded nanofiber dressing improves wound healing in diabetic mice. *Eur J Pharm Sci*. 2018;121:269–280. doi:10.1016/j.ejps.2018.05.031
3. Patel S, Srivastava S, Singh MR, Singh D. Mechanistic insight into diabetic wounds: pathogenesis, molecular targets and treatment strategies to pace wound healing. *Biomed Pharmacother*. 2019;112:108615. doi:10.1016/j.biopha.2019.108615
4. Bernal-Chavez S, Nava-Arzaluz MG, Quiroz-Segoviano RIY, Ganem-Rondero A. Nanocarrier-based systems for wound healing. *Drug Dev Ind Pharm*. 2019;45(9):1389–1402.
5. Mihai MM, Dima MB, Dima B, Holban AM. Nanomaterials for wound healing and infection control. *Materials*. 2019;12(13):1.
6. Han G, Ceilley R. Chronic wound healing: a review of current management and treatments. *Adv Ther*. 2017;34(3):599–610.
7. Manford AG, Mena EL, Shih KY, et al. Structural basis and regulation of the reductive stress response. *Cell*. 2021;184(21):5375–5390.
8. Rotariu D, Babes EE, Tit DM, et al. Oxidative stress - Complex pathological issues concerning the hallmark of cardiovascular and metabolic disorders. *Biomed Pharmacother*. 2022;152:113238.
9. Dunnill C, Patton T, Brennan J, et al. Reactive oxygen species (ROS) and wound healing: the functional role of ROS and emerging ROS-modulating technologies for augmentation of the healing process. *Int Wound J*. 2017;14(1):89–96.
10. Weavers H, Wood W, Martin P. Injury activates a dynamic cytoprotective network to confer stress resilience and drive repair. *Curr Biol*. 2019;29 (22):3851–3862. doi:10.1016/j.cub.2019.09.035
11. Long L, Liu W, Hu C, Yang L, Wang Y. Construction of multifunctional wound dressings with their application in chronic wound treatment. *Biomater Sci*. 2022;10(15):4058–4076. doi:10.1039/D2BM00620K
12. Ribeiro CT, Dias FA, Fregonezi GA. Hydrogel dressings for venous leg ulcers. *Cochrane Database Syst Rev*. 2022;8:CD010738.
13. Milan EP, Martins VCA, Horn MM, Plepis AMG. Influence of blend ratio and mangosteen extract in chitosan/collagen gels and scaffolds: rheological and release studies. *Carbohydr Polym*. 2022;292:119647. doi:10.1016/j.carbpol.2022.119647
14. Schiefer JL, Aretz GF, Fuchs PC, et al. Comparison of wound healing and patient comfort in partial-thickness burn wounds treated with SUPRATHEL and epicte (hydro) wound dressings. *Int Wound J*. 2022;19(4):782–790. doi:10.1111/iwj.13674
15. Gaspar-Pintiliescu A, Stanciuc AM, Craciunescu O. Natural composite dressings based on collagen, gelatin and plant bioactive compounds for wound healing: a review. *Int J Biol Macromol*. 2019;138:854–865. doi:10.1016/j.ijbiomac.2019.07.155
16. Chattopadhyay S, Raines RT. Review collagen-based biomaterials for wound healing. *Biopolymers*. 2014;101(8):821–833. doi:10.1002/bip.22486
17. Pieper JS, van der Kraan PM, Hafmans T, et al. Crosslinked type II collagen matrices: preparation, characterization, and potential for cartilage engineering. *Biomaterials*. 2002;23(15):3183–3192. doi:10.1016/S0142-9612(02)00067-4
18. Guo R, Lan Y, Xue W, et al. Collagen-cellulose nanocrystal scaffolds containing curcumin-loaded microspheres on infected full-thickness burns repair. *J Tissue Eng Regen Med*. 2017;11(12):3544–3555. doi:10.1002/term.2272
19. Jimenez RA, Millan D, Suesca E, Sosnik A, Fontanilla MR. Controlled release of an extract of Calendula officinalis flowers from a system based on the incorporation of gelatin-collagen microparticles into collagen I scaffolds: design and in vitro performance. *Drug Deliv Transl Res*. 2015;5 (3):209–218. doi:10.1007/s13346-015-0217-3
20. Wang Y, Cao Z, Wei Q, et al. VH298-loaded extracellular vesicles released from gelatin methacryloyl hydrogel facilitate diabetic wound healing by HIF-1alpha-mediated enhancement of angiogenesis. *Acta Biomater*. 2022;147:342–355. doi:10.1016/j.actbio.2022.05.018
21. Santoro M, Tatara AM, Mikos AG. Gelatin carriers for drug and cell delivery in tissue engineering. *J Control Release*. 2014;190:210–218. doi:10.1016/j.jconrel.2014.04.014
22. Cha C, Shin SR, Annabi N, Dokmeci MR, Khademhosseini A. Carbon-based nanomaterials: multifunctional materials for biomedical engineering. *ACS Nano*. 2013;7(4):2891–2897. doi:10.1021/nn401196a
23. Lee C, Wei X, Kysar JW, Hone J. Measurement of the elastic properties and intrinsic strength of monolayer graphene. *Science*. 2008;321 (5887):385–388. doi:10.1126/science.1157996
24. Li X, Zhu Y, Cai W, et al. Transfer of large-area graphene films for high-performance transparent conductive electrodes. *Nano Lett*. 2009;9 (12):4359–4363. doi:10.1021/nl902623y
25. Nair M, Nancy D, Krishnan AG, Anjusree GS, Vadukumpully S, Nair SV. Graphene oxide nanoflakes incorporated gelatin-hydroxyapatite scaffolds enhance osteogenic differentiation of human mesenchymal stem cells. *Nanotechnology*. 2015;26(16):161001. doi:10.1088/0957-4484/26/16/161001
26. Paul A, Hasan A, Kindi HA, et al. Injectable graphene oxide/hydrogel-based angiogenic gene delivery system for vasculogenesis and cardiac repair. *ACS Nano*. 2014;8(8):8050–8062. doi:10.1021/nn5020787
27. Jiao D, Wang J, Yu W, et al. Biocompatible reduced graphene oxide stimulated BMSCs induce acceleration of bone remodeling and orthodontic tooth movement through promotion on osteoclastogenesis and angiogenesis. *Bioact Mater*. 2022;15:409–425. doi:10.1016/j.bioactmat.2022.01.021
28. Shen C, Liu J, Lu Q, Wang G, Wang Z, Liu L. Pre-vascularized electrospun graphene oxide-gelatin chamber for intestinal wall defect repair. *Int J Nanomedicine*. 2022;17:681–695. doi:10.2147/IJN.S353029
29. Lasram MM, Dhouib IB, Annabi A, El Fazaa S, Gharbi N. A review on the possible molecular mechanism of action of N-acetylcysteine against insulin resistance and type-2 diabetes development. *Clin Biochem*. 2015;48(16–17):1200–1208. doi:10.1016/j.clinbiochem.2015.04.017
30. Atkuri KR, Mantovani JJ, Herzenberg LA, Herzenberg LA. N-Acetylcysteine–a safe antidote for cysteine/glutathione deficiency. *Curr Opin Pharmacol*. 2007;7(4):355–359. doi:10.1016/j.coph.2007.04.005
31. Oguz A, Uslukaya O, Alabalik U, Turkoglu A, Kapan M, Bozdag Z. Topical N-acetylcysteine improves wound healing comparable to dexpanthenol: an experimental study. *Int Surg*. 2015;100(4):656–661. doi:10.9738/INTSURG-D-14-00227.1
32. Tsai ML, Huang HP, Hsu JD, et al. Topical N-acetylcysteine accelerates wound healing in vitro and in vivo via the PKC/Stat3 pathway. *Int J Mol Sci*. 2014;15(5):7563–7578. doi:10.3390/ijms15057563
33. Tugba Camic B, Oytun F, Hasan Aslan M, Jeong Shin H, Choi H, Basarir F. Fabrication of a transparent conducting electrode based on graphene/ silver nanowires via layer-by-layer method for organic photovoltaic devices. *J Colloid Interface Sci*. 2017;505:79–86. doi:10.1016/j.jcis.2017.05.065
34. Wang J, Wu D, Zhang Z, et al. Biomimetically ornamented rapid prototyping fabrication of an apatite-collagen-polycaprolactone composite construct with Nano-Micro-Macro hierarchical structure for large bone defect treatment. *ACS Appl Mater Interfaces*. 2015;7(47):26244–26256.
35. Liu J, Hou J, Liu S, et al. Graphene oxide functionalized double-layered patch with anti-adhesion ability for abdominal wall defects. *Int J Nanomedicine*. 2021;16:3803–3818. doi:10.2147/IJN.S312074

36. Wang X, Ge J, Tredget EE, Wu Y. The mouse excisional wound splinting model, including applications for stem cell transplantation. *Nat Protoc*. 2013;8(2):302–309.
37. Nascimento-Filho CHV, Silveira EJD, Goloni-Bertollo EM, de Souza LB, Squarize CH, Castilho RM. Skin wound healing triggers epigenetic modifications of histone H4. *J Transl Med*. 2020;18(1):138.
38. Somanathan T, Prasad K, Ostrikov KK, Saravanan A, Krishna VM. Graphene oxide synthesis from agro waste. *Nanomaterials*. 2015;5(2):826–834.
39. Li J, Zhou C, Luo C, et al. N-acetyl cysteine-loaded graphene oxide-collagen hybrid membrane for scarless wound healing. *Theranostics*. 2019;9(20):5839–5853.
40. Song R, Murphy M, Li C, Ting K, Soo C, Zheng Z. Current development of biodegradable polymeric materials for biomedical applications. *Drug Des Devel Ther*. 2018;12:3117–3145.
41. Echave MC, Saenz del Burgo L, Pedraz JL, Orive G. Gelatin as biomaterial for tissue engineering. *Curr Pharm Des*. 2017;23(24):3567–3584.
42. Sartuqui J, Gravina AN, Rial R, et al. Biomimetic fiber mesh scaffolds based on gelatin and hydroxyapatite nano-rods: designing intrinsic skills to attain bone reparation abilities. *Colloids Surf B Biointerfaces*. 2016;145:382–391.
43. Kim TH, Shah S, Yang L, et al. Controlling differentiation of adipose-derived stem cells using combinatorial graphene hybrid-pattern arrays. *ACS Nano*. 2015;9(4):3780–3790.
44. Lafuente-Merchan M, Ruiz-Alonso S, Garcia-Villen F, et al. 3D bioprinted hydroxyapatite or graphene oxide containing nanocellulose-based scaffolds for bone regeneration. *Macromol Biosci*. 2022;2022:e2200236.
45. Zhang Y, Ouyang H, Lim CT, Ramakrishna S, Huang ZM. Electrospinning of gelatin fibers and gelatin/PCL composite fibrous scaffolds. *J Biomed Mater Res B Appl Biomater*. 2005;72(1):156–165.
46. Ramanathan G, Muthukumar T, Tirichurapalli Sivagnanam U. In vivo efficiency of the collagen coated nanofibrous scaffold and their effect on growth factors and pro-inflammatory cytokines in wound healing. *Eur J Pharmacol*. 2017;814:45–55.
47. Singaravelu S, Ramanathan G, Sivagnanam UT. Dual-layered 3D nanofibrous matrix incorporated with dual drugs and their synergetic effect on accelerating wound healing through growth factor regulation. *Mater Sci Eng C Mater Biol Appl*. 2017;76:37–49.
48. Jurgelene Z, Montvydiene D, Semcuk S, et al. The impact of co-treatment with graphene oxide and metal mixture on Salmo trutta at early development stages: the sorption capacity and potential toxicity. *Sci Total Environ*. 2022;838(Pt 4):156525.
49. Bachle AC, Morsdorf P, Rezaeian F, Ong MF, Harder Y, Menger MD. N-acetylcysteine attenuates leukocytic inflammation and microvascular perfusion failure in critically ischemic random pattern flaps. *Microvasc Res*. 2011;82(1):28–34.
50. Paskal W, Kopka M, Stachura A, et al. Single dose of N-Acetylcysteine in local anesthesia increases expression of HIF1alpha, MAPK1, TGFbeta1 and growth factors in rat wound healing. *Int J Mol Sci*. 2021;22(16):1.